Drug Design, Development and Therapy

Dovepress
Taylor & Francis Group

Open Access Full Text Article

ORIGINAL RESEARCH

Mechanistic Physiologically Based Pharmacokinetic Modeling to Predict CYP3A4-Mediated Drug–Drug Interactions of Flumatinib as Both a Victim and a Perpetrator

Muyesaier Alifu[1,*], Xue Chu[2,*], Xinyan Zhu[1], Wen Yao Mak[1], Aole Zheng[1], Chunyang Pan[1], Qingfeng He[1], Xiao Zhu[1], Zheng Kuai[3], Xiaoqiang Xiang[1]

[1]Department of Clinical Pharmacy and Pharmacy Administration, School of Pharmaceutical Sciences, Fudan University, Shanghai, People's Republic of China; [2]Department of Oncology, The Second Affiliated Hospital of Soochow University, Suzhou, Jiangsu, People's Republic of China; [3]Department of Geriatrics, Zhongshan Hospital, Fudan University, Shanghai, People's Republic of China

*These authors contributed equally to this work

Correspondence: Zheng Kuai, Department of Geriatrics, Zhongshan Hospital, Fudan University, Shanghai, 200032, People's Republic of China, Email kuai.zheng@zs-hospital.sh.cn; Xiaoqiang Xiang, Department of Clinical Pharmacy and Pharmacy Administration, School of Pharmaceutical Sciences, Fudan University, Shanghai, 201203, People's Republic of China, Email xiangxq@fudan.edu.cn

Background: Flumatinib is an orally administered tyrosine kinase inhibitor (TKI) that selectively targets the BCR-ABL fusion protein and is approved in China for treating adult patients with chronic-phase chronic myeloid leukemia (CML-CP). It is mainly metabolized by CYP3A4 and CYP2C8 and exhibits time-dependent inhibition (TDI) of CYP3A4. However, its clinical drug–drug interaction (DDI) potential remains insufficiently characterized.

Methods: A series of in vitro experiments were conducted using human liver microsomes and Caco-2 cells to characterize the pharmacokinetic properties of flumatinib, including CYP3A4 time-dependent inhibition and key physicochemical inputs relevant to systemic disposition. These data, together with in silico estimates and clinical pharmacokinetic profiles, were integrated into a mechanistic physiologically based pharmacokinetic (PBPK) model for Chinese subjects. Predictive performance was assessed by comparing simulated and clinically observed exposure ratios.

Results: The PBPK model demonstrated robust performance, with predicted-to-observed exposure ratios predominantly within the 0.5–2.0-fold range. DDI simulations indicated that, as a perpetrator, flumatinib exerted minimal impact on CYP3A4 substrate exposure. However, when acting as a victim, co-administration with strong CYP3A4 inhibitors (itraconazole, ketoconazole) increased flumatinib $AUC_{0\text{-}72h}$ by approximately 12-fold (AUCR = 11.65–12.96), whereas rifampicin decreased C_{max} and $AUC_{0\text{-}72h}$ by 2.4- and 4.7-fold ($C_{max}R$ = 0.41, AUCR = 0.21), respectively.

Conclusion: Flumatinib shows negligible perpetrator potential but is highly sensitive to CYP3A4 modulation. PBPK-informed DDI assessment supports cautious co-administration with strong CYP3A4 inhibitors or inducers and guides its rational clinical use.

Keywords: flumatinib, PBPK model, drug–drug interaction, CYP3A4 inhibitor, CYP3A4 inducer

Introduction

Chronic myeloid leukemia (CML) is a rare hematologic malignancy with an annual incidence of approximately 1–2 cases per 100,000 people.[1–3] In 2017, China ranked among the top three countries globally in terms of CML incidence, with 2999.5 new cases reported, highlighting its considerable disease burden.[4] CML is an age-related neoplasm, with a median age at diagnosis of about 60 years in Western countries, whereas patients in Africa and Asia are typically diagnosed nearly a decade earlier.[5] In China, the combination of a relatively younger patient population and a high incidence translates into a substantial and sustained treatment demand, highlighting the need for more effective and accessible therapeutic options.

https://doi.org/10.2147/DDDT.S574169
Received: 15 October 2025
Accepted: 15 April 2026
Published: 9 May 2026

Over the past decade, BCR-ABL1 tyrosine kinase inhibitors (TKIs) have revolutionized the first-line treatment of chronic-phase Philadelphia chromosome-positive (Ph+) chronic myeloid leukemia (CML-CP). Many patients with CML-CP respond well to first-line TKI therapy, including imatinib and second-generation TKIs (bosutinib, dasatinib, and nilotinib). However, resistance remains a challenge for a subset of patients.[6] Imatinib resistance has also been documented in China, with a multicenter study across 15 hospitals reporting rates of 6.87% in outpatients and 16.28% in inpatients. Notably, the resistance profile differed between settings: secondary resistance predominated in outpatients, while primary resistance was more frequent among inpatients.[7]

Flumatinib Mesylate (HH-GV-678) is a novel selective BCR-ABL1 inhibitor that effectively suppresses BCR-ABL1 activity, overcomes imatinib resistance caused by BCR-ABL1 point mutations, and demonstrates superior efficacy to imatinib both in vitro and in vivo.[8] In an unpublished Phase 2 study, both flumatinib 400 mg and 600 mg exhibited significantly higher rate of major molecular response (MMR) compared with imatinib in newly diagnosed CML-CP.[9] The randomized Phase III trial involving 394 newly diagnosed CML-CP Chinese patients also show that flumatinib (600 mg once daily) demonstrated significantly superior efficacy compared to imatinib (400 mg once daily), with higher rates of early molecular response (EMR) at 3 months (82.1% vs. 53.3%) and MMR at 6 and 12 months (33.7% vs. 18.3% and 52.6% vs. 39.6%, respectively).[10] While safety profiles were overall comparable, fewer hematologic and non-hematologic adverse events (AEs) were observed with flumatinib. These findings support its clinical advantage and has led to its approval by the China National Medical Products Administration (NMPA) in November 2019 for the treatment of adult patients with Ph+ CML.[11]

Enzyme kinetic studies have identified CYP3A4 and CYP2C8 as the primary enzymes involved in flumatinib metabolism.[12] In vitro drug-drug interaction (DDI) studies using human liver microsomes (HLM) and recombinant enzymes demonstrated that CYP3A4 inhibitors—such as erythromycin, cyclosporine, voriconazole, and isavuconazole—significantly inhibited flumatinib metabolism.[13] Correspondingly, in vivo pharmacokinetic studies in rats showed increased plasma concentrations and systemic exposure of flumatinib following co-administration with these inhibitors.[12,13] According to its prescribing information, flumatinib also exhibits time-dependent inhibition (TDI) of CYP3A4.[14] Despite evidence of metabolic interactions in preclinical studies, no clinical DDI investigations of flumatinib have been conducted to date. Therefore, a comprehensive evaluation of its interaction potential in humans is essential to guide dose optimization and enhance treatment safety.

DDI represents a clinically significant concern for TKIs in CML treatment. For instance, co-administration of imatinib with strong CYP3A4 inhibitors such as ketoconazole increases its exposure by approximately 40%, while inducers like rifampicin reduce exposure by up to 74%, potentially compromising therapeutic efficacy or increasing toxicity risk.[15] These observations underscore the importance of proactive DDI assessment for newly developed TKIs to guide rational clinical use.

Current DDI assessment follows a stepwise strategy recommended by regulatory agencies, beginning with in vitro experiments and mechanistic static models, progressing to dynamic PBPK simulations when warranted, thereby reducing reliance on dedicated clinical DDI studies.[16,17] China's NMPA has issued a DDI study guideline that is closely aligned with FDA (Food and Drug Administration) and EMA (European Medicines Agency) frameworks in both in vitro and clinical study requirements, reflecting the broader harmonization of China's drug regulatory landscape with international standards.[18]

Physiologically based pharmacokinetic (PBPK) modeling is a mechanistic framework that quantitatively predicts the in vivo absorption, distribution, metabolism, and excretion (ADME) of drugs using physiological parameters and compound physicochemical properties.[19] Notably, PBPK modeling has been widely used in developing small-molecule targeted anticancer agents, providing insights into their pharmacokinetics and supporting enzyme-mediated DDI assessment and dose optimization.[20,21] Its predictive power is increasingly recognized by regulatory agencies such as the FDA and EMA, which actively support its application in drug development and clinical DDI risk assessment.[22,23] In this study, a PBPK model for flumatinib was developed and verified to predict its DDI potential both as a perpetrator and a victim drug to further support its rational clinical use.

Materials and Methods

CYP3A4/CYP2C8 Stability Assay

Intrinsic clearance of flumatinib was determinate from CYP3A4/CYP2C8 Stability Assay. Flumatinib was purchased from Shanghai YuanYe Bio-Technology Co., Ltd. (China), with batch number C12O11L126689. Recombinant CYP3A4

enzyme was purchased from Corning (New York, USA) with batch numbers 1313003 and recombinant CYP2C8 enzyme was obtained from Cypex (Dundee, UK) with the batch number of C2C8R008A.

Intrinsic clearance ($CL_{int,\ CYP3A4}$) was determined through a substrate consumption assay. Working solutions of the test compound (flumatinib) and the positive control (midazolam) were prepared using acetonitrile (ACN) at concentrations of 100 μM and 200 μM, respectively. NADPH was dissolved in phosphate-buffered saline (PBS, pH 7.4) to achieve a final concentration of 2 mM. The pre-incubation mixture included the test compound or positive control, $MgCl_2$ (6 mM), recombinant CYP3A4 enzyme (2000 pmol/mL), and PBS, which was pre-incubated at 37°C for 5 minutes. Samples were incubated for 0, 5, 15, 30, and 60 minutes (15 minutes for positive control). The reactions were terminated by adding ACN containing internal standard. All samples were mixed for 5 minutes at 6°C and centrifuged at *5500 x g* for 10 minutes. Approximately 150 μL of supernatant was analyzed by LC-MS/MS. For the determination of CYP2C8 intrinsic clearance ($CL_{int,\ CYP2C8}$), the same procedure was followed, except that amodiaquine replaced midazolam as the positive control. Detailed LC-MS/MS parameters can be found in Tables S1 and 2.

For the enzymes CYP3A4 and CYP2C8, the remaining percentage of the substrate was calculated according to equation (1), with the initial concentration set as 100%. The intrinsic clearance (CL_{int}, mL/min/pmol) for recombinant CYP3A4 and CYP2C8 was subsequently determined using Equation (2).

$$percentage\ remaining(\%) = \left\{ \frac{Average\left[\left(\frac{A_T}{A_{IS}}\right)_{t_n}\right]}{Average\left[\left(\frac{A_T}{A_{IS}}\right)_{t_0}\right]} \right\} \times 100\% \tag{1}$$

$$CL_{int}(mL/min/pmol) = \frac{k}{c} \tag{2}$$

A_T and A_{IS} represent the peak areas of the test compound and the internal standard, respectively. t_n and t_0 denote the non-zero incubation time points and the zero-minute incubation time point, respectively. In equation (2), the k is representing the elimination rate constant and c is the concentration of recombinant enzyme.

Blood to Plasma (B/P) Ratio Assay

Human whole blood and plasma samples used for the B/P ratio assay were obtained from healthy donors. Flumatinib stock solutions (10 mM) were prepared in DMSO and stored at −20°C. A 100 μM working solution was obtained by diluting the stock in 80% acetonitrile/water. Human whole blood was pre-warmed at 37°C for 10 min prior to dosing. For baseline (0 h) sampling, 10 μL of the 20 μM flumatinib working solution was added to 190 μL of whole blood, vortexed, and 50 μL was immediately collected. For incubation, 5 μL of the 20 μM working solution was added to 95 μL of whole blood to achieve a final concentration of 1 μM. The samples were incubated at 37°C for 1 h, after which 50 μL of whole blood was taken as the 1 h whole-blood sample. The remaining blood was centrifuged at 1,900 × *g* for 10 min to obtain plasma, and 50 μL of plasma was collected as the 1 h plasma sample.

For sample preparation, 50 μL of whole blood or plasma (or 20 μL of plasma, depending on assay conditions) was mixed with internal standard-containing acetonitrile. The mixture was vortexed thoroughly and centrifuged at 15,700 × *g* for 10 minutes. A 150 μL aliquot of the supernatant was transferred into a 96-well plate, diluted with 150 μL of ultrapure water, and subjected to LC–MS/MS analysis as described above. The blood-to-plasma concentration ratio (B/P) was calculated using the following equation (3–5):

$$B/PRatio = C_b/C_P \tag{3}$$

$$C_r/C_p = 2C_b/C_p - 1 \tag{4}$$

$$Recovery(\%) = C_b/C_{b0} \tag{5}$$

In the equation, C_b, C_p, and C_r represent the concentrations in whole blood, plasma, and red blood cells, respectively, after 1 hour of incubation, while C_{b0} represents the whole blood concentration at 0 hours.

Caco-2 Permeability Assay

The Caco-2 cell line was sourced from the Cell Resource Center, Shanghai Institutes for Biological Sciences, Chinese Academy of Sciences. Firstly, Caco-2 Cells were seeded onto 96-well Transwell plate at a density of 1.0–2.0 × 10^5 cells/cm^2 and cultured for 15 to 28 days prior to the experiment, with the medium replaced every 1 to 3 days. The transfer buffer consisted of Hanks' Balanced Salt Solution (HBSS) supplemented with 10 mM 4-(2-hydroxyethyl)-1-piperazineethanesulfonic acid (HEPES), adjusted to pH 7.4. Test compounds, including minoxidil, atenolol, digoxin, and flumatinib, were diluted with the transfer buffer to a concentration of 5 μM. Bidirectional transport was evaluated in the apical-to-basolateral (A→B) and basolateral-to-apical (B→A) directions. For A→B, 75 μL of donor solution was added to the apical chamber and 250 μL of receiver buffer to the basolateral chamber; the setup was reversed for B→A. The plates were incubated at 37°C for 120 min. Following incubation, samples were mixed with a termination solution containing internal standard. The integrity of the cell monolayer membrane after transport was evaluated by measuring fluorescein leakage. The concentrations of test and reference compounds were quantified using LC-MS/MS analysis (Table S3). The apparent permeability coefficient (P_{app}, unit: ×10^{-6} cm/s) was calculated using equation (6):

$$P_{app} = (dC_r/dt) \times V_r/(A \times C_0) \tag{6}$$

Where dC_r/dt represents the rate of change in cumulative drug concentration in the receiver compartment over time; V_r denotes the volume of the solution in the receiver compartment (0.075 mL for the apical side and 0.25 mL for the basolateral side); A is the surface area of the cell monolayer (0.0804cm^2); and C_0 is the initial concentration in the donor compartment.

Time-Dependent Inhibition in Human Liver Microsomes (HLMs)

A two-step incubation method was used to evaluate the TDI of CYP3A4 by flumatinib, using the metabolism of testosterone to 6β-hydroxytestosterone in HLMs as the probe reaction. Flumatinib stock solutions were prepared in DMSO and further diluted with phosphate-buffered saline (PBS) to generate a concentration gradient (12.3, 37.0, 111, 333, and 1000 μM). The experiment included a test group (TG), in which flumatinib was added, and a negative control (NC) group, in which an equal volume of vehicle was used. In the TG, flumatinib was pre-incubated with HLMs (4.00 mg/mL) and NADPH (4.00 mM) at 37°C for 0, 5, 15, 30, and 60 minutes. After pre-incubation, the reaction mixtures were diluted 10-fold with PBS containing testosterone (250 μM) and NADPH and incubated again at 37°C for 10 minutes to assess residual CYP3A4 activity. The reaction was terminated by transferring 100 μL of the incubation mixture into 400 μL of ice-cold methanol containing an internal standard. The NC group was processed in the same manner as the TG. All samples were vortexed, centrifuged to precipitate proteins, and the supernatants were collected for quantification of 6β-hydroxytestosterone using LC–MS/MS (Table S4). The relative enzyme activity at each inhibitor concentration was calculated as equation 7:

$$Relative\ Activity(\%ofNC) = \left(\frac{Metabolite\ Peak\ Area\ Ratio\ of\ Test\ Group}{Metabolite\ Peak\ Area\ Ratio\ of\ Negative\ Control\ Group}\right) \times 100 \tag{7}$$

The remaining enzyme activity (%) was calculated based on the amount of probe metabolite formed at each pre-incubation time point. The natural logarithm of the remaining activity was plotted against incubation time to obtain the observed inactivation rate constant (K_{obs}), which corresponds to the negative slope of the linear regression line. Subsequently, K_{obs} values (min^{-1}) were plotted against flumatinib concentrations (μM) to estimate the TDI parameters. Both nonlinear regressions based on the Michaelis–Menten model and Lineweaver–Burk linear fitting ($1/K_{obs}$ vs. 1/[I]) were performed using GraphPad Prism to determine the maximum inactivation rate constant (k_{inact}) and the inactivator concentration at half-maximal inactivation (K_I).

$$k_{obs} = \frac{k_{inact} \times [I]}{K_I + [I]} \tag{8}$$

k_{obs} represents the observed inactivation rate constant (min^{-1}), *[I]* denotes the inhibitor concentration (μM), k_{inact} is the maximal inactivation rate constant, and K_I refers to the inhibitor concentration at which half-maximal inactivation is achieved.

Model Development and Parameter Acquisition

A full PBPK model of flumatinib was developed using GastroPlus® (modeling software) version 9.9 (Simulations Plus, Inc., Lancaster, CA, USA). The DDI module was utilized to assess the TDI potential of flumatinib and to simulate its interactions with CYP3A4 inhibitors and inducers. PBPK models for interacting compounds were constructed and verified within the modeling software. Key model parameters of flumatinib are summarized in Table 1, with additional details provided in Table S5. Virtual individuals were generated using the Population Estimates for Age-Related (PEAR) Physiolog™ module in the modeling software. Demographic characteristics considered during model construction included: (1) the average age, body weight, or body

Table 1 Core Parameters Used for the Construction of the Flumatinib PBPK Model

Parameters	Value	Source
Physicochemical parameters		
Molecular weight (g/mol)	562.6	Drug bank
log P	4.132	Predicted by ADMET Predictor™
Solubility at pH 9.03 (mg/mL)	0.08753	Predicted by ADMET Predictor™
Compound type	Diprotic Base	
pK_a	10.72	Predicted by ADMET Predictor
	7.92	
Rbp	1.46	In vitro experiments
$f_{u,p}$ (%)	4.04	Lipid adjusted by the modeling software
Absorption parameters	ACAT Model	
Caco-2 permeability (10^{-6} cm·s^{-1})	0.15	In vitro experiments
$f_{u,G}$	1	Assumed
Formulation	Immediate Release (IR) Tablet	
Dissolution model	Johnson	The modeling software default value
Distribution parameters	Full PBPK Model	
V_{ss} (L)	562.99	Predicted by the modeling software
K_P method		The modeling software default (Lukacova)
Elimination parameters		
Systemic clearance, CL_{sys} (L/h)	12.6	Predicted by the modeling software
$CL_{int\ CYP3A4}$ (μL/min/pmol)	4.31	In vitro experiments
$CL_{int\ CYP2C8}$ (μL/min/pmol)	3.62	In vitro experiments
$K_{m,\ (rCYP3A4)}$ (μM)	3.06	Liu, et al2023[13]
Interaction		
$K_{I-\ CYP3A4}$ (μM)	197.6	In vitro experiment
$k_{inact-\ CYP3A4}$(1/min)	0.0192	In vitro experiment

Abbreviations: log P, partition coefficient in oil and water; pK_a, acid dissociation constant; *Rbp*: Blood to Plasma concentration ratio; $f_{u,p}$, unbound fraction in plasma; $f_{u,G}$, unbound fraction in gut; F_a, Fraction Absorbed; V_{ss}, volume of distribution at steady-state; CL_{int}, intrinsic clearance; K_I, concentration of mechanism-based inhibitor associated with half maximal inactivation rate; K_{inact}, maximal inactivation rate constant of the enzyme;

https://doi.org/10.2147/DDDT.S574169

mass index (BMI) of study subjects; (2) sex distribution, with a male-specific model used when the number of males was equal to or greater than that of females; and (3) the fasting or fed status of subjects.[24]

Physicochemical properties, such as the octanol/water partition coefficient (log P) and dissociation constant (pK_a), were predicted using ADMET Predictor® (Simulations Plus, Inc., Lancaster, CA, USA) version 10.4 based on the chemical structure of flumatinib. According to the drug label, the average plasma protein binding in humans is approximately 89.4%.[14] Given that disease states such as chronic myeloid leukemia (CML) are known to alter plasma protein levels—particularly through increased concentrations of α-1-acid glycoprotein (AAG),[25–27] the unbound fraction in plasma ($f_{u,p}$) was subsequently lipid-adjusted using the modeling software, yielding a final value of 4.04%. This adjusted $f_{u,p}$ was used as the model input and provided improved agreement between the simulated and observed plasma concentration–time profiles. Flumatinib was formulated as an immediate-release (IR) tablet, and the in vitro dissolution profile was modeled using the Johnson dissolution function.

The Advanced Compartmental Absorption and Transit (ACAT™) model was used to describe gastrointestinal absorption. Absorption scaling factors (ASFs) were initially predicted using the default Opt logD model (SA/V 6.1) and then refined to match observed excretion data. Considering that <1% of flumatinib is excreted in urine and ~20% is recovered unchanged in feces,[28] ASF values were optimized using a user-defined model to yield an estimated F_a of ~80% (Table S5). The effective permeability (P_{eff}) was based on Caco-2 assay results. Paracellular permeability was incorporated using the default Zhimin method implemented in the modeling software.[29] To simulate a worst-case intestinal DDI scenario, the fraction of unbound drug in the gut ($f_{u,G}$) was assumed to be 1.0. The blood-to-plasma concentration ratio (B/P) was determined to be 1.46 from in vitro experiments.

Flumatinib is extensively distributed throughout the body, with a large apparent volume of distribution.[14,30] The whole-body PBPK model in the modeling software was used to characterize tissue distribution. A perfusion-limited distribution model was applied to all tissues, and tissue-to-plasma partition coefficients (K_p) were predicted using the Lukacova method (Rodgers single-adjustment algorithm).[30] For the elimination module, previous pharmacokinetic studies reported that only 0.504 ± 0.3% of the administered flumatinib dose is excreted unchanged in urine, and approximately 20% is excreted unchanged in feces,[28] suggesting that hepatic metabolism is the primary elimination route. The intrinsic clearance values of flumatinib via CYP3A4 and CYP2C8 ($CL_{int,CYP3A4}$ and $CL_{int,CYP2C8}$) were obtained from in vitro enzyme incubation studies and subsequently scaled to in vivo values using the Metabolism & Transport module of the modeling software (Table S5).

As the primary aim of this study was to evaluate CYP3A4-mediated drug–drug interactions, and only the in vitro K_m of flumatinib in recombinant CYP3A4 (rCYP3A4, K_m = 3.06 μM) has been reported,[13] we further estimated in vivo enzyme kinetics based on the scaled $CL_{int,CYP3A4}$. Using the Metabolism & Transport module of the modeling software, in vivo K_m and V_{max} values were fitted and incorporated into the PBPK model to quantitatively describe CYP3A4-mediated metabolism. These parameters were essential for simulating CYP3A4 related DDI scenarios.

Model Verification

Three independent clinical studies were used to verify the model, covering single-dose and multiple-dose regimens as well as different sampling durations, to ensure robust predictive performance (Table S6). For model development, verification and simulations, virtual *Chinese healthy Subjects* under fasted condition were generated (25 subjects). The gender distribution was set to be equal, with both male and female values assigned as 0.5.

For each simulation trial, the area under the concentration-time curve (AUC) and maximum plasma concentration (C_{max}) ratio were reported as arithmetic mean ratio. AUC values were calculated from the time of drug administration to the time of the last concentration measurement (AUC_{last}). The predictive performance of PBPK models is evaluated using the Fold Error (FE) of the AUC and C_{max} as shown in Equation 9. FE is considered acceptable when the ratios fall within the predefined success range (0.5–2-fold).[31] Goodness-of-fit (GOF) plots for model evaluation were generated using R software (version 4.4.3). In addition, the visual inspection checks were deemed acceptable if the clinically determined plasma concentrations are within the 10^{th} and 90^{th} percentiles of the predicted profile.[20,32]

$$Fold\ error(FE) = \frac{predicted\ PK\ value}{Observed\ PK\ value} \tag{9}$$

Model Application

After model verification, the PBPK model was employed to simulate DDIs involving flumatinib as both a perpetrator and a victim. To evaluate flumatinib's potential as a perpetrator of CYP3A4-mediated interactions, simulations were conducted using representative CYP3A4 substrates—midazolam, alfentanil, and triazolam—whose PBPK models were independently constructed and verified within the modeling software. In these simulations, flumatinib was administered once daily for 10 consecutive days, while the CYP3A4 substrate was administered on Day 8 after 7 days of flumatinib dosing, by which time flumatinib ($t_{1/2}$ approximately 16–17 h) had reached steady-state concentrations and maximal CYP3A4 inactivation, consistent with the simulation design reported for ensartinib.[9,19] To assess flumatinib as a victim drug, co-administration scenarios with typical CYP3A4 inhibitors (itraconazole, fluconazole, ketoconazole, and N-demethyl Diltiazem) and inducers (rifampin and efavirenz) were simulated. The PBPK models for these interacting compounds, which are predefined in the modeling software, were also verified prior to the simulations. In this setting, the perpetrator drug was administered for 10 days, and flumatinib was given on Day 8. Specific dosing regimens for all drugs involved in the simulations are provided in Table S7. DDI magnitude was evaluated based on the arithmetic mean ratios (with vs. without flumatinib or perpetrator) of C_{max} and AUC_{last}, calculated using Equations (10) and (11).

$$AUC_{ratio} = \frac{AUC\ with\ inhibitor\ or\ inducer}{AUC\ without\ inhibitor\ or\ inducer} \tag{10}$$

$$C_{\max ratio} = \frac{C_{max} with\ inhibitor\ or\ inducer}{C_{max} without\ inhibitor\ or\ inducer} \tag{11}$$

Ethics Statement

The mechanistic PBPK model fitting and subsequent validation were conducted using drug concentration data exclusively extracted from previously published studies; therefore, these processes did not require independent ethical approval or new recruitment of human participants. To derive critical parameters for model construction, a blood-to-plasma (B/P) ratio assay was conducted using blank human blood samples from healthy volunteers. This experimental work was approved by the Ethics Committee of Changsha Nanya Hospital for Clinical Trial Medical Research (Ethics Approval No. (2023) 035). The assay itself was subsequently performed by an external contracted laboratory. Written informed consent was obtained from all volunteers prior to sample collection, in accordance with the Declaration of Helsinki. All blood specimens were fully anonymized to protect donor privacy.

Results

In vitro Experiments

Metabolic stability assays were conducted using recombinant CYP3A4 and CYP2C8 enzymes. The residual parent concentrations over time are presented in Table S8 and the metabolic clearance profiles are shown in Figure S1. The estimated intrinsic clearance (CL_{int}) values were 0.00431 mL/min/pmol for CYP3A4 and 0.00362 mL/min/pmol for CYP2C8 (Table S9). The experimentally determined blood-to-plasma concentration ratio (Rbp) was 1.46 (Table S10). Flumatinib exhibited low permeability in the Caco-2 assay, with an apparent A-to-B P_{app} of 0.15×10^{-6} cm/s, and showed marked polarized transport (B-to-A/A-to-B ratio = 124), suggesting possible involvement of intestinal efflux transporters such as P-glycoprotein (P-gp) or breast cancer resistance protein (BCRP) (Table S11). While the current study focuses on metabolic interaction potential, the effective human jejunal permeability (P_{eff}) was also estimated using the default Zhimin method in the modeling software, yielding a value of 0.23×10^{-4} cm/s. TDI of CYP3A4 by flumatinib was further evaluated in HLM using testosterone as the probe substrate. The TDI kinetic parameters were determined to be K_I = 197.6 μM and k_{inact} = 0.0192 min^{-1} (Table S12 and Figure S2).

https://doi.org/10.2147/DDDT.S574169

PBPK Model Validation

The PBPK model was validated under multiple clinical scenarios to evaluate its predictive performance for flumatinib pharmacokinetics. As shown in Figures 1 and 2, the majority of observed plasma concentration–time data fell within the 10^{th} to 90^{th} percentile prediction intervals for both single- and multiple-dose regimens. GOF plots showed that 86.1% of the predicted-to-observed concentration ratios after single-dose administration fell within the 0.5–2-fold acceptance range (Figure 3A). For multiple-dose simulations, the proportions within this range were 94.6% with TDI and 82.1% without TDI, indicating an improved predictive performance after incorporation of TDI mechanism (Figure 3B and C). Detailed comparisons of predicted versus observed PK parameters are provided in Table 2 (single dose) and Table 3 (multiple dose). Under multiple-dose conditions, the model without TDI tended to underpredict flumatinib exposure in some regimens, whereas incorporation of TDI resulted in better overall agreement with the observed data and more reasonably characterized the moderate accumulation of flumatinib at steady state.

Sensitivity analysis identified the unbound plasma fraction ($f_{u,p}$) as a key parameter influencing model performance. Considering the elevated *α1*-acid glycoprotein levels commonly observed in patients with CML, $f_{u,p}$ was adjusted to 0.04. This refinement notably improved the model's predictive accuracy, particularly under multiple-dose conditions. Following parameter optimization, the predicted C_{max} and AUC_{0-t} values across the 80–600 mg dose range fell within the predefined acceptance criteria for both single- and multiple-dose simulations.

PBPK Model Application

When flumatinib was evaluated as a perpetrator, its potential to affect the pharmacokinetics of sensitive CYP3A4 substrates was assessed in simulated healthy Chinese volunteers. Flumatinib was administered for 10 days, with midazolam, alfentanil, or triazolam dosed on Day 8 (Table S7). As shown in Figure 4 and Table 4, the simulation results suggested minimal to moderate changes in substrate exposure, indicating a low perpetrator risk.

When flumatinib was evaluated as a victim, its interaction with representative CYP3A4 inhibitors and inducers was simulated under the same dosing schedule (Table S7). Co-administration with strong CYP3A4 inhibitors, itraconazole and ketoconazole, resulted in marked increases in flumatinib exposure, with predicted C_{max} and AUC_{0-72h} elevated by up to ~10-fold and ~12-fold, respectively. Moderate inhibitors such as fluconazole and N-demethyl diltiazem also led to

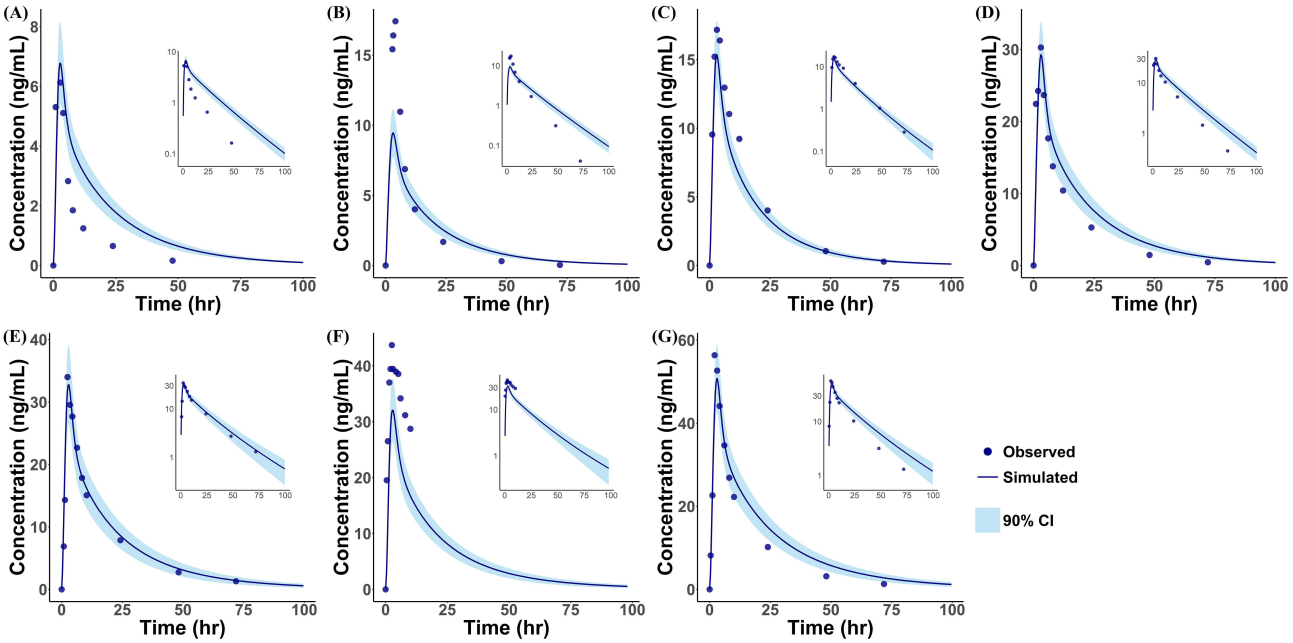

Figure 1 Model validation: observed and simulated mean plasma concentration–time profiles of flumatinib after single-dose administration in healthy Chinese subjects. **(A)** 80 mg, **(B)** 140 mg, **(C)** 240 mg, **(D)** 360 mg (Gong study); **(E)** 400 mg (Bojiang study), **(F)** 400 mg (Kuang study), **(G)** 600 mg (Bojiang study). Blue circles indicate observed concentrations, solid lines indicate simulated concentrations, and shaded areas indicate the 90% confidence intervals. Insets show the semi-logarithmic plots.

https://doi.org/10.2147/DDDT.S574169

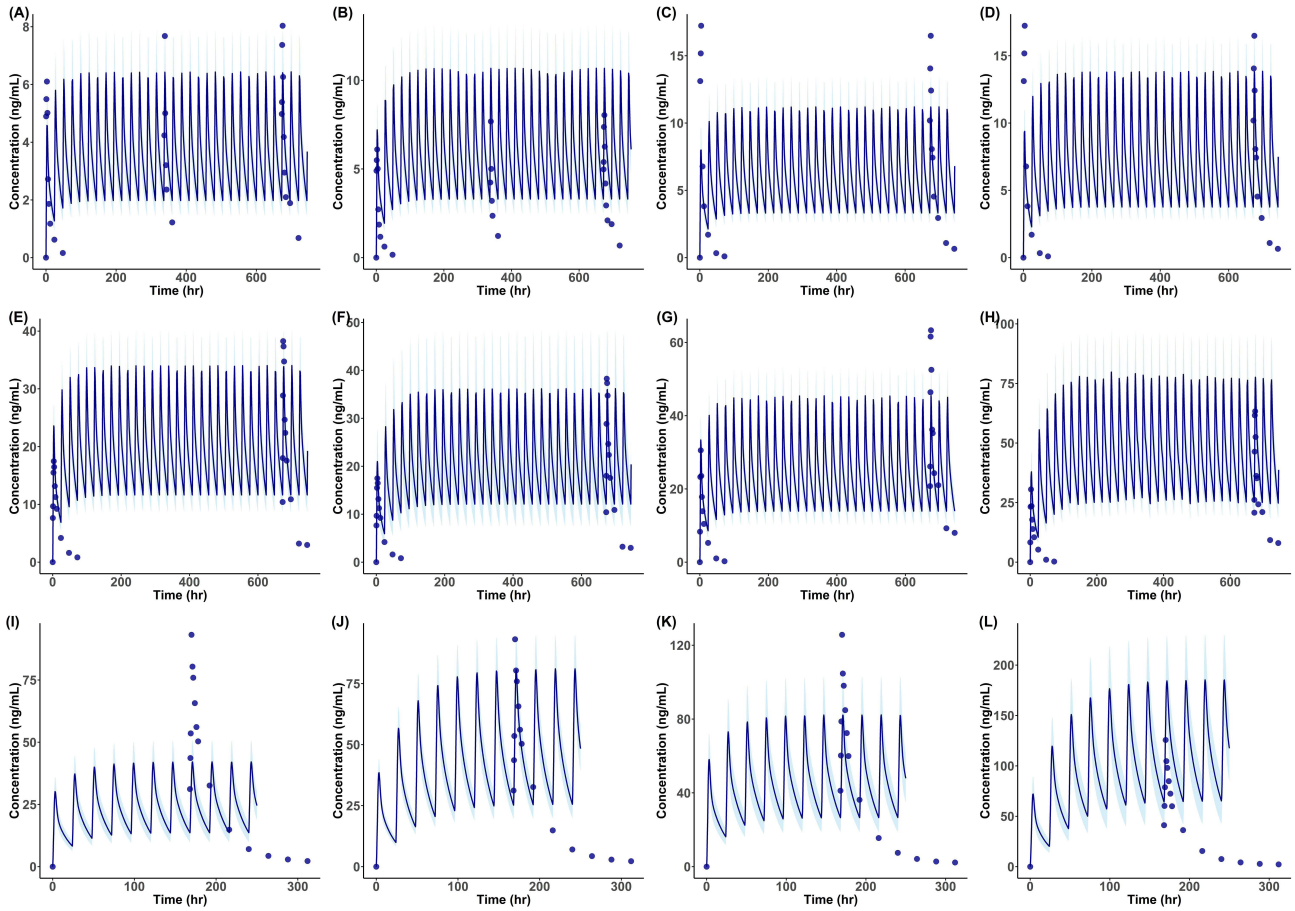

Figure 2 Model validation: observed and simulated mean plasma concentration–time profiles of flumatinib during multiple-dose administration with and without incorporation of TDI. (**A**) Gong 80 mg once daily without TDI; (**B**) Gong 80 mg once daily with TDI; (**C**) Gong 140 mg once daily without TDI; (**D**) Gong 140 mg once daily with TDI; (**E**) Gong 240 mg once daily without TDI; (**F**) Gong 240 mg once daily with TDI; (**G**) Gong 360 mg once daily without TDI; (**H**) Gong 360 mg once daily with TDI; (**I**) Bojiang 400 mg once daily without TDI; (**J**) Bojiang 400 mg once daily with TDI; (**K**) Bojiang 600 mg once daily without TDI; and (**L**) Bojiang 600 mg once daily with TDI. Blue circles indicate observed concentrations, solid lines indicate simulated concentrations, and shaded areas indicate the 90% confidence intervals.

substantial increases in exposure, with C_{max} and $AUC_{0–72h}$ ratios ranging from 5.88 to 8.68 and 8.71 to 13.53, respectively (Figure 4 and Table 5). In contrast, co-administration with the strong CYP3A4 inducer rifampin significantly reduced flumatinib exposure, with predicted C_{max} and $AUC_{0–72h}$ decreased by 2.42-fold and 4.67-fold, respectively. Efavirenz, a moderate inducer, had a negligible effect on flumatinib pharmacokinetics (Figure 4 and Table 5).

Discussion

To our knowledge, this is the first study to integrate in vitro CYP3A4 inhibition data with mechanistic PBPK modeling to characterize flumatinib as both a perpetrator and a victim of CYP3A4-mediated DDIs in humans. Despite limited prior data that were mainly derived from rat models and focused solely on its victim role, no studies have evaluated flumatinib's perpetrator effects or its DDI potential in humans.[12,13] To address this gap, we incorporated in vitro TDI kinetics into the PBPK model, alongside in vivo-fitted K_m and V_{max} values for CYP3A4 based on scaled intrinsic clearance data. The final model adequately described the pharmacokinetics of flumatinib under single and multiple dosing conditions, with predictions predominantly within accepted performance criteria, and successfully predicted its interaction potential with typical CYP3A4 substrates and modulators. These findings provide mechanistic insight into flumatinib's metabolic behavior and offer a predictive framework to guide its rational clinical use, inform DDI risk management, and support regulatory decision-making.

During PBPK model development, several refinements were required because of limited compound-specific data.[25–27] In this study, a lipid-adjusted $f_{u,p}$ of 0.04 was used based on the modeling software prediction and verified via sensitivity

https://doi.org/10.2147/DDDT.S574169

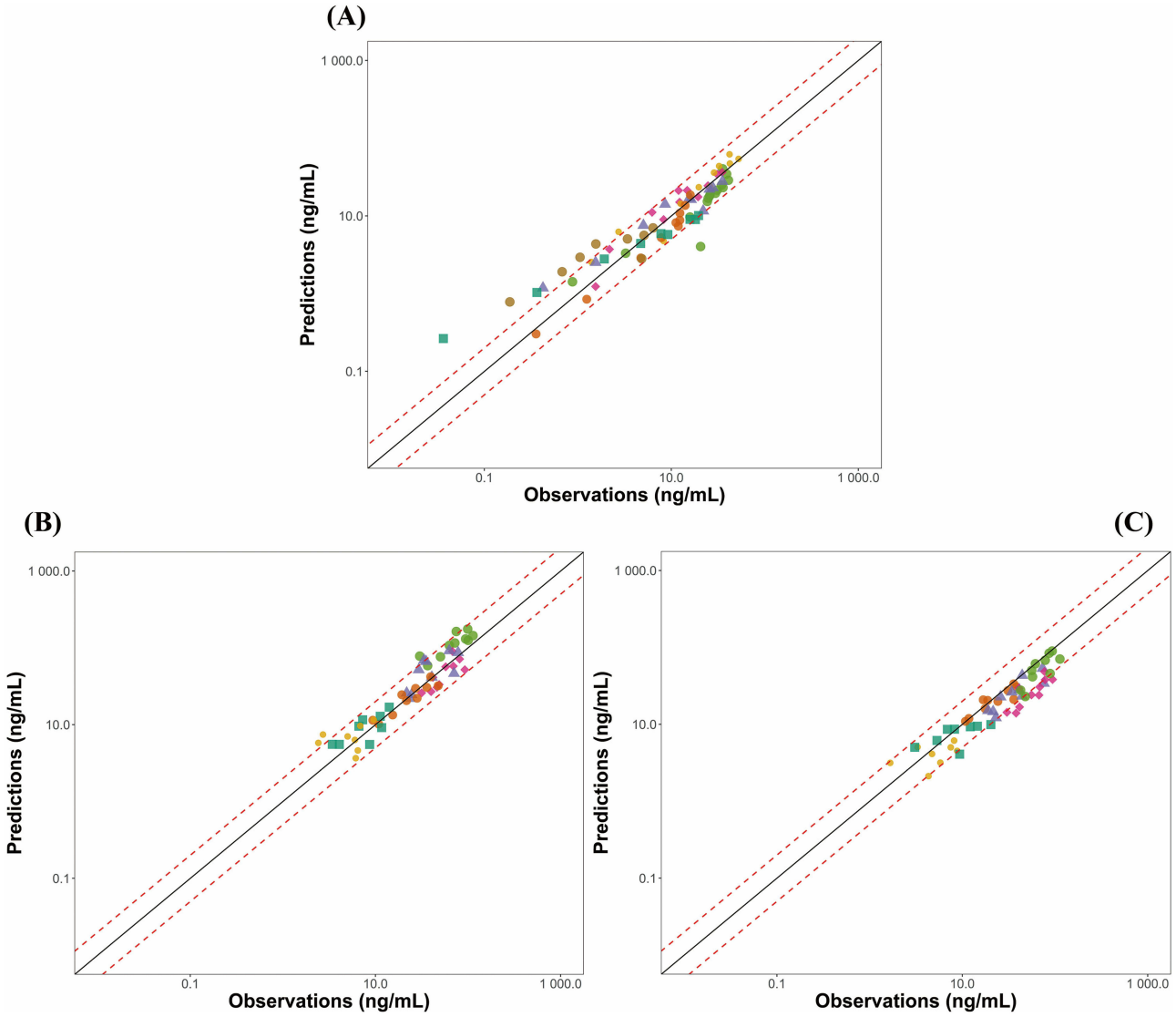

Figure 3 Goodness-of-fit plots for the final flumatinib PBPK model. (**A**) Single-dose flumatinib; (**B**) multiple-dose flumatinib with TDI; and (**C**) multiple-dose flumatinib without TDI. Different symbols indicate different dose groups. In (**A**) the dose groups were 80, 140, 240, 360, 400, and 600 mg. In (**B** and **C**) the dose groups were 80, 140, 240, 360, 400, and 600 mg once daily. The solid black line indicates the line of identity, and the red dashed lines indicate the 2-fold deviation boundaries.

analysis, which demonstrated acceptable model performance under both single- and multiple-dose conditions. Accordingly, the current model is expected to remain applicable to Chinese healthy subjects and to patients with CML who have generally preserved hepatic function. Extrapolation to other populations, particularly patients with hepatic impairment, should be made cautiously, as altered physiology may affect systemic exposure and potentially modify the magnitude of CYP3A4-mediated DDIs. In addition, the marked polarized transport in Caco-2 assays suggested possible involvement of intestinal efflux transporters. Therefore, absorption scaling factors (ASFs) were adjusted using a user-defined model based on the available metabolism and clinical excretion data for flumatinib.[28,34] Finally, flumatinib exposure has been reported to be affected by a high-fat meal.[33] Accordingly, the current simulations were conducted under fasted conditions, consistent with the package insert recommendation and clinical use. Extrapolation of these predictions to fed conditions should therefore be made cautiously.

The current PBPK model demonstrated good predictive performance across a wide dose range (80–600 mg) under both single- and multiple-dose conditions, with nearly all simulated C_{max} and AUC_{0-t} values falling within the accepted 2-fold error range. A slight underprediction was noted in the 140 mg single-dose study by Gong et al,[28] likely due to high

Table 2 Observed and Predicted Pharmacokinetic Parameters of Flumatinib After Single-Dose Administration

Dosing Regimens	Parameters	Observed	Predicted	FE
80mg single dose, fasted (Gong et al, 2010, n = 3)[28]	C_{max} (ng/mL)	6.8 ± 1.01	7.22	1.06
	AUC_{0-t} (ng·h/mL)	57.8 ± 16.0[a]	124.92	2.16
140mg single dose, fasted (Gong et al, 2010, n = 6)[28]	C_{max} (ng/mL)	29.6 ± 27.4	10.15	0.34
	AUC_{0-t} (ng·h/mL)	201 ± 165 [a]	170.10	0.85
240mg single dose, fasted (Gong et al, 2010, n = 3)[28]	C_{max} (ng/mL)	18.6 ± 8.7	16.54	0.89
	AUC_{0-t} (ng·h/mL)	321 ± 222 [a]	243.67	0.76
360mg single dose, fasted (Gong et al, 2010, n = 3)[28]	C_{max} (ng/mL)	32.4 ± 4.7	30.21	0.93
	AUC_{0-t} (ng·h/mL)	414 ± 102 [a]	535.45	1.29
400mg single dose, fasted (Bojiang et al, 2023, n= 15)[9]	C_{max} (ng/mL)	38.0 ± 12.5	34.9	0.92
	AUC_{0-t} (ng·h/mL)	536.3 ±179.9 [a]	597.46	1.11
400mg single dose, fasted (Kuang et al, 2020, n=12)[33]	C_{max} (ng/mL)	50.7 ± 32.5	35.90	0.71
	AUC_{0-t} (ng·h/mL)	832 ± 566[b]	585.97	0.70
600mg single dose, fasted (Bojiang et al, 2023, n=14)[9]	C_{max} (ng/mL)	61.9 ± 50.0	53.60	0.87
	AUC_{0-t} (ng·h/mL)	746.7 ± 534.7[a]	998.82	1.34

Abbreviations: C_{max}, maximum plasma concentration; AUC_{0-t}, Area Under the Curve from time 0 to t; a: Area Under the Curve from time 0 to 72h; b: Area Under the Curve from time 0 to 96h; FE, Fold Error.

Table 3 Observed and Predicted Pharmacokinetic Parameters of Flumatinib After Multiple-Dose Administration with/Without CYP3A4 Time-Dependent Inhibition (TDI)

Dosing Regimens	Parameters	Observed	With Auto-Inhibition		Without Auto-Inhibition	
			Predicted	FE	Predicted	FE
80mg qd, Days 1–28, fasted (Gong et al, 2010, n = 3)[28]	C_{max} (ng/mL)	8.04	10.68	1.33	6.41	0.80
	AUCss (ng·h/mL)	53.28	100.68	1.89	59.23	1.11
140mg qd, Days 1–28, fasted (Gong et al, 2010, n=6)[28]	C_{max} (ng/mL)	16.49	13.82	0.84	11.19	0.68
	AUCss (ng·h/mL)	155.29	174.83	1.13	148.59	0.96
240mg qd, Days 1–28, fasted (Gong et al,2010, n=3)[28]	C_{max} (ng/mL)	38.26	35.99	0.94	33.86	0.88
	AUCss (ng·h/mL)	480.35	500.47	1.04	472.31	0.98
360mg qd, Days 1–28, fasted (Gong et al, 2010, n=3)[28]	C_{max} (ng/mL)	63.33	77.60	1.23	45.45	0.72
	AUCss (ng·h/mL)	752.38	1080.16	1.44	588.99	0.78
400mg qd, Days 4–11, fasted (Bojiang et al, 2023, n=15)[9]	C_{max} (ng/mL)	93.17	80.75	0.87	42.07	0.45
	AUCss (ng·h/mL)	1224.76	1087.11	0.89	568.38	0.46
600mg qd, Days 4–11, fasted (Bojiang et al, 2023, n=14)[9]	C_{max} (ng/mL)	125.67	184.35	1.47	82.14	0.65
	AUCss (ng·h/mL)	1500.89	2614.49	1.74	1100.51	0.73

Abbreviations: C_{max}, maximum plasma concentration; AUC_{ss}, calculating the Area Under the Curve with NCA method (one complete dosing interval at steady state); FE, Fold Error.

https://doi.org/10.2147/DDDT.S574169

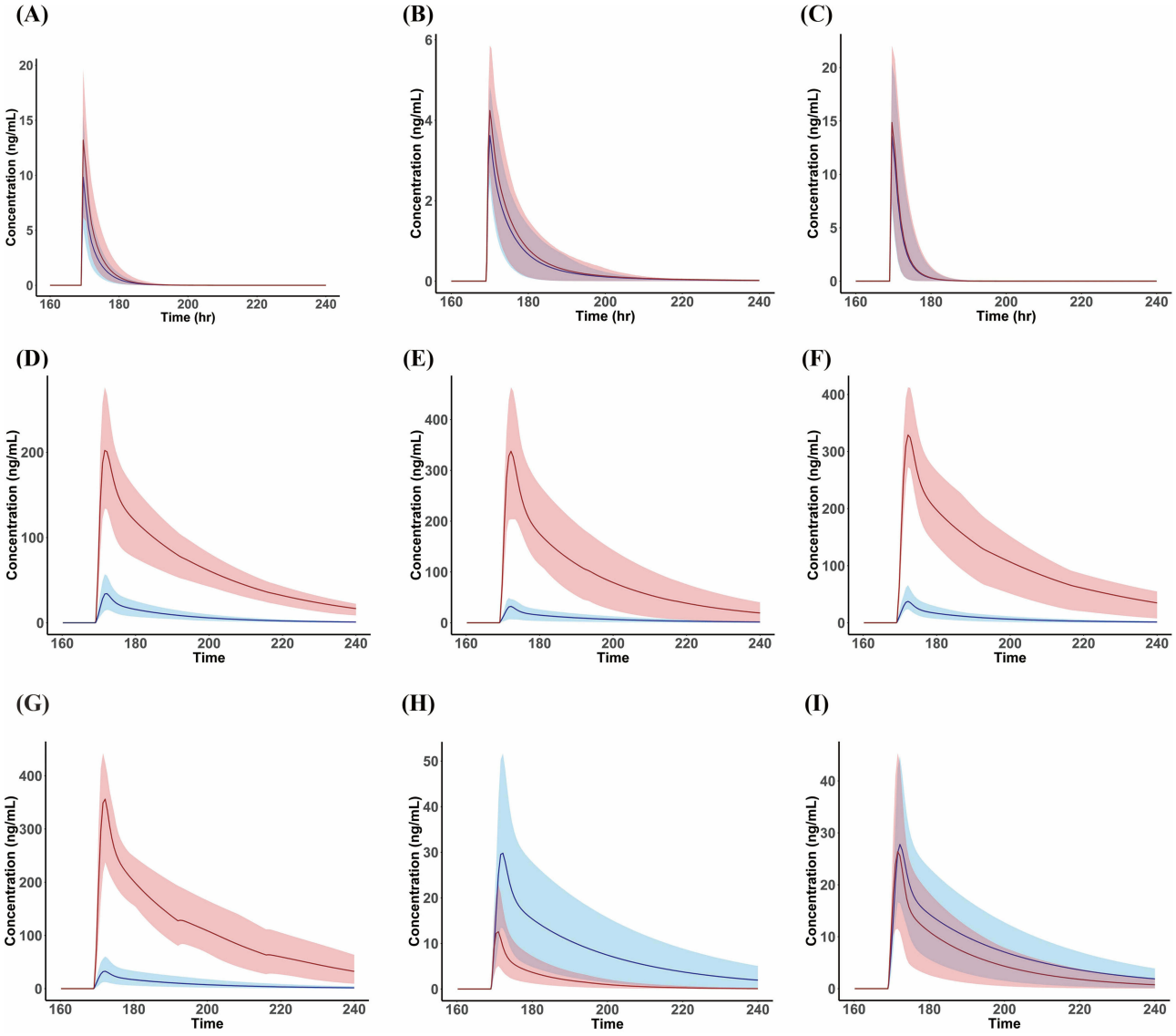

Figure 4 Predicted CYP3A4-mediated drug–drug interactions involving flumatinib in simulated healthy Chinese subjects. Blue lines and shaded areas represent the predicted concentration–time profiles of flumatinib or CYP3A4 substrate drugs when administered alone, whereas red lines and shaded areas represent the corresponding profiles during co-administration with the interacting drugs. (**A**–**C**) show flumatinib as a perpetrator with the CYP3A4 substrates midazolam, triazolam, and alfentanil, respectively. (**D**–**G**) show flumatinib as a victim with the CYP3A4 inhibitors fluconazole, itraconazole, N-demethyldiltiazem, and ketoconazole, respectively. (**H**–**I**) show flumatinib as a victim with the CYP3A4 inducers rifampin and efavirenz, respectively.

inter-individual variability (C_{max}: 29.6 ± 27.4 ng/mL; AUC_{0-t}: 201 ± 16 ng·h/mL; n = 6). Under multiple-dose conditions, clinical data showed a 3- to 4-fold increase in exposure at steady state, indicating moderate accumulation without statistical significance.[9] Incorporating TDI parameters (K_I: 197.6 μM; k_{inact}: 0.0192 min^{-1}) improved model predictions and better captured observed PK profiles under repeated dosing. Simulated accumulation ratios for C_{max} and AUC generally ranged from 0.5- to 2-fold compared with single-dose exposure, with a mild dose-dependent trend but no significant differences, consistent with clinical findings.[9] The lack of marked accumulation suggested no clear evidence of CYP3A4 saturation within the studied dose range, likely due to the limited extent of TDI, and was generally consistent with approximately linear pharmacokinetics of flumatinib under the evaluated conditions.

In DDI simulations, flumatinib exhibited a moderate effect on the pharmacokinetics of typical CYP3A4 substrates, including midazolam, alfentanil, and triazolam. Co-administration led to increases in C_{max} and AUC values within 1.5-fold, suggesting that flumatinib, as a perpetrator, is unlikely to require dose adjustment of co-administered CYP3A4 substrates. However, as flumatinib is primarily metabolized by CYP3A4, it may also act as a victim in DDIs. While

Table 4 Predicted Pharmacokinetics of CYP3A4 Substrates Co-Administered with Flumatinib in Simulated Healthy Chinese Subjects

Substrate	Parameters	Unit	Substrate Alone	Substrate + Flumatinib	Ratio
Midazolam (5mg single dose)	C_{max}	ng/mL	10.00	13.60	1.36
	AUC_{0-72h}	ng·h/mL	34.69	48.90	1.41
Alfentanil (1.065mg single dose)	C_{max}	ng/mL	13.90	15.20	1.10
	AUC_{0-72h}	ng·h/mL	40.89	45.15	1.11
Triazolam (0.5mg single dose)	C_{max}	ng/mL	3.70	4.30	1.16
	AUC_{0-72h}	ng·h/mL	25.14	29.90	1.19

Note: AUC_{0-72h}: area under the plasma concentration–time curve from time 0 to 72h; C_{max}, maximum plasma concentration.

Table 5 Predicted Pharmacokinetic Parameters of 400 mg Flumatinib Administered Alone or Co-Administered with CYP3A4 Inhibitors and Inducers

Co-Administered Drugs		Parameters	Unit	Chinese Healthy Populations		
				Flumatinib Alone	Combined	Ratio
Inhibitors	Itraconazole 200mg qd	C_{max}	ng/mL	33.00	343.20	10.40
		AUC_{0-72h}	ng·h/mL	562.02	6550.20	11.65
	Ketoconazole 400mg qd	C_{max}	ng/mL	33.70	368.10	10.92
		AUC_{0-72h}	ng·h/mL	621.39	8052.70	12.96
	Fluconazole 400mg qd	C_{max}	ng/mL	35.00	204.70	5.88
		AUC_{0-72h}	ng·h/mL	535.40	4660.70	8.71
	N-demethyl Diltiazem 100mg qd	C_{max}	ng/mL	38.20	331.70	8.68
		AUC_{0-72h}	ng·h/mL	589.34	7975.70	13.53
Inducers	Rifampicin 600mg qd	C_{max}	ng/mL	31.40	13.00	0.41
		AUC_{0-72h}	ng·h/mL	593.87	127.30	0.21
	Efavirenz 400mg qd	C_{max}	ng/mL	28.20	26.70	0.92
		AUC_{0-72h}	ng·h/mL	556.44	396.44	0.66

Abbreviations: AUC_{0-72h}, area under the plasma concentration–time curve from time 0 to 72h; C_{max}, maximum plasma concentration; qd, once daily drug administration.

previous preclinical studies in rats have shown increased flumatinib exposure when co-administered with erythromycin or cyclosporine,[12] our PBPK simulations provided a human-specific perspective. Co-administration with strong CYP3A4 inhibitors (eg., itraconazole, ketoconazole) and moderate inhibitors (eg., N-demethyl diltiazem, fluconazole) resulted in more than a 5-fold increase in flumatinib C_{max} and AUC, whereas co-administration with strong inducers (eg., rifampin) reduced exposure by 2.4- to 4.7-fold. According to the FDA M12 Drug Interaction Studies: Guidance for Industry, these interactions fall into the strong and moderate DDI categories, respectively.[17] These human-based predictions highlight the need for clinical caution, as excessive or subtherapeutic exposures may compromise safety or efficacy. Therefore, dose adjustments or avoidance of co-administration should be considered when flumatinib is used with strong CYP3A4 modulators, as substantial changes in flumatinib exposure may affect treatment effectiveness or tolerability.

This study has several limitations. First, several clinical datasets used for model verification had relatively small sample sizes and substantial inter-individual variability, which may increase the uncertainty of the observed PK estimates

and corresponding fold-error calculations. Second, although Caco-2 assays suggested possible involvement of intestinal efflux transporters, transporter-mediated processes were not explicitly incorporated into the current PBPK model, which may limit the accuracy of absorption- and distribution- related predictions. Third, CYP3A4 enzyme kinetics were estimated by reverse-fitting in vivo clearance data because in vivo K_m and V_{max} values were unavailable, which may introduce additional variability and uncertainty. Finally, because no human DDI studies involving flumatinib are currently available, the predicted DDIs could not be externally validated and should therefore be interpreted as model-based projections rather than clinically confirmed effects. Future studies should prospectively evaluate these predicted interactions in clinically relevant settings, particularly with strong CYP3A4 inhibitors and inducers, and further refine translation between the current in vitro conditions and clinically relevant in vivo exposure scenarios.

Conclusion

In conclusion, we developed and validated a PBPK model for flumatinib integrating in vitro data and clinical pharmacokinetic observations from Chinese subjects. The model reasonably captured flumatinib's dual role as a time-dependent inhibitor and a sensitive substrate of CYP3A4, providing mechanistic insights into its potential DDIs. These findings offer a rationale for dose optimization and risk management in patients with CML, supporting informed co-administration with CYP3A4 substrates, inhibitors, and inducers. Moreover, the study highlights the utility of PBPK modeling in predicting DDI risks and guiding clinical and regulatory decisions for oncology therapeutics. Prospective clinical studies are warranted to validate these predictions and further refine dosing strategies in patient populations.

Data Sharing Statement

The authors declare that all the data supporting the findings of this study are available within the paper and its Supplemental Materials.

Acknowledgments

We thank all the contributors for their invaluable contributions to this article.

Funding

This study was supported by the National Natural Science Foundation of China and the National Research Foundation of Korea (No. 82011540409).

Disclosure

The authors declared no potential conflicts of interest in this work.

References

1. Osman AEG, Deininger MW. Chronic myeloid leukemia: modern therapies, current challenges and future directions. *Blood Rev*. 2021;49:100825. doi:10.1016/j.blre.2021.100825
2. Hehlmann R, Hochhaus A, Baccarani M. Chronic myeloid leukaemia. *Lancet*. 2007;370(9584):342–350. doi:10.1016/s0140-6736(07)61165-9
3. Cortes J, Pavlovsky C, Saußele S. Chronic myeloid leukaemia. *Lancet*. 2021;398(10314):1914–1926. doi:10.1016/s0140-6736(21)01204-6
4. Ning L, Hu C, Lu P, Que Y, Zhu X, Li D. Trends in disease burden of chronic myeloid leukemia at the global, regional, and national levels: a population-based epidemiologic study. *Exp Hematol Oncol*. 2020;9(1):29. doi:10.1186/s40164-020-00185-z
5. Mendizabal AM, Younes N, Levine PH. Geographic and income variations in age at diagnosis and incidence of chronic myeloid leukemia. *Int J Hematol*. 2016;103(1):70–78. doi:10.1007/s12185-015-1893-y
6. Malik S, Hassan S, Eşkazan AE. Novel BCR-ABL1 tyrosine kinase inhibitors in the treatment of chronic myeloid leukemia. *Expert Rev Hematol*. 2021;14(11):975–978. doi:10.1080/17474086.2021.1990034
7. Wang JX, Huang XJ, Wu DP, Hu JD, Huang HH. Overview of chronic myelogenous leukemia and its current diagnosis and treatment patterns in 15 hospitals in China. *Zhonghua xue ye xue za zhi*. 2009;30(11):721–725.
8. Luo H, Quan H, Xie C, Xu Y, Fu L, Lou L. HH-GV-678, a novel selective inhibitor of Bcr-Abl, outperforms imatinib and effectively overrides imatinib resistance. *Leukemia*. 2010;24(10):1807–1809. doi:10.1038/leu.2010.169
9. Jiang B, Qi J, Sun M, et al. Pharmacokinetics of single- and multiple-dose flumatinib in patients with chronic phase chronic myeloid leukemia. *Front Oncol*. 2023;13:1101738. doi:10.3389/fonc.2023.1101738
10. Zhang L, Meng L, Liu B, et al. Flumatinib versus imatinib for newly diagnosed chronic phase chronic myeloid leukemia: a phase III, randomized, open-label, multi-center FESTnd study. *Clin Cancer Res*. 2021;27(1):70–77. doi:10.1158/1078-0432.Ccr-20-1600

11. (NMPA) NMPA. Flumatinib mesylate approved for the treatment of chronic myeloid leukemia. Available from: https://www.nmpa.gov.cn/directory/web/nmpa//zhuanti/cxylqx/cxypxx/20191126142301880.html. Accessed September 11, 2024.
12. Chen J, Guo S, Yu X, et al. Metabolic interactions between flumatinib and the CYP3A4 inhibitors erythromycin, cyclosporine, and voriconazole. *Die Pharmazie*. 2020;75(9):424–429. doi:10.1691/ph.2020.0068
13. Liu YN, Xu X, Nie J, et al. Studies on the inhibitory effect of isavuconazole on flumatinib metabolism in vitro and in vivo. *Front Pharmacol*. 2023;14:1168852. doi:10.3389/fphar.2023.1168852
14. (NMPA) NMPA. Flumatinib mesylate tablets: prescribing information. Available from: https://cn.hspharm.com/upload/file/2023/03/06/3799f766d8f4494aa0a44bd073f05bb0.pdf. Accessed September 15, 2024.
15. Haouala A, Widmer N, Duchosal MA, Montemurro M, Buclin T, Decosterd LA. Drug interactions with the tyrosine kinase inhibitors imatinib, dasatinib, and nilotinib. *Blood*. 2011;117(8):e75–87. doi:10.1182/blood-2010-07-294330
16. Polli JE. In vitro studies are sometimes better than conventional human pharmacokinetic in vivo studies in assessing bioequivalence of immediate-release solid oral dosage forms. *AAPS J*. 2008;10(2):289–299. doi:10.1208/s12248-008-9027-6
17. Administration FaD. M12 drug interaction studies guidance for industry. Available from: https://www.fda.gov/regulatory-information/search-fda-guidance-documents/m12-drug-interaction-studies. Accessed Feb 05, 2025.
18. Tang W, Huang Y, Zhou D, et al. Evolving drug regulatory landscape in China: a clinical pharmacology perspective. *Clin Transl Sci*. 2021;14(4):1222–1230. doi:10.1111/cts.12987
19. Wang X, Yu Y, Liu H, et al. Prediction of drug-drug interactions with ensartinib as a time-dependent CYP3A inhibitor using physiologically based pharmacokinetic model. *Drug Metab Dispos*. 2023;51(11):1515–1526. doi:10.1124/dmd.123.001373
20. Min JS, Bae SK. Prediction of drug-drug interaction potential using physiologically based pharmacokinetic modeling. *Arch Pharm Res*. 2017;40(12):1356–1379. doi:10.1007/s12272-017-0976-0
21. Wang X, Chen F, Guo N, et al. Application of physiologically based pharmacokinetics modeling in the research of small-molecule targeted anti-cancer drugs. *Cancer Chemother Pharmacol*. 2023;92(4):253–270. doi:10.1007/s00280-023-04566-z
22. Administration USFD. Physiologically based pharmacokinetic analyses—format and content. Available from: https://www.fda.gov/drugs/guidance-compliance-regulatory-information/guidances-drugs. Accessed May 20, 2025.
23. European Medicines Agency: London U. Guideline on the reporting of physiologically based pharmacokinetic (PBPK) modelling and simulation. 2018.
24. Yin X, Cicali B, Rodriguez-Vera L, Lukacova V, Cristofoletti R, Schmidt S. Applying physiologically based pharmacokinetic modeling to interpret carbamazepine's nonlinear pharmacokinetics and its induction potential on cytochrome P450 3A4 and cytochrome P450 2C9 enzymes. *Pharmaceutics*. 2024;16(6). doi:10.3390/pharmaceutics16060737
25. De Zwart L, Snoeys J, Jacobs F, et al. Prediction of the drug-drug interaction potential of the α1-acid glycoprotein bound, CYP3A4/CYP2C9 metabolized oncology drug, erdafitinib. *CPT Pharmacometrics Syst Pharmacol*. 2021;10(9):1107–1118. doi:10.1002/psp4.12682
26. Song L, Guo H, Wang L. Relationship between serum α1-acid glycoprotein, imatinib concentration, and therapeutic efficacy in patients with chronic myeloid leukemia. *J Qiqihar Med Univer*. 2016;27(12).
27. Zhong J, Meng F, Xu D, Dai M, Wei Y, Zhou H. Relationship between serum α1-acid glycoprotein, imatinib concentration, and therapeutic efficacy in patients with chronic myeloid leukemia. *Chinese Med J*. 2011;91(30):4.
28. Gong A. *Pharmacokinetics and Metabolism of Flumatinib in Patients with Chronic Myeloid Leukemia*. Graduate University of Chinese Academy of Sciences; 2010.
29. Zhimin H. Estimation of Paracellular Drug Permeability Through Cell Monolayers. *Transactions of Tianjin University*. 1995;1(1):42–47.
30. Schmitt W. General approach for the calculation of tissue to plasma partition coefficients. *Toxicol in vitro*. 2008;22(2):457–467. doi:10.1016/j.tiv.2007.09.010
31. Zheng A, Yang D, Pan C, et al. Modeling the complexity of drug-drug interactions: a physiologically-based pharmacokinetic study of Lenvatinib with Schisantherin A/Schisandrin A. *Eur J Pharm Sci*. 2024;196:106757. doi:10.1016/j.ejps.2024.106757
32. Kuepfer L, Niederalt C, Wendl T, et al. Applied concepts in PBPK modeling: how to build a PBPK/PD model. *CPT Pharmacometrics Syst Pharmacol*. 2016;5(10):516–531. doi:10.1002/psp4.12134
33. Kuang Y, Song HL, Yang GP, et al. Effect of high-fat diet on the pharmacokinetics and safety of flumatinib in healthy Chinese subjects. *Cancer Chemother Pharmacol*. 2020;86(3):339–346. doi:10.1007/s00280-020-04117-w
34. Gong A, Chen X, Deng P, Zhong D. Metabolism of flumatinib, a novel antineoplastic tyrosine kinase inhibitor, in chronic myelogenous leukemia patients. *Drug Metab Dispos*. 2010;38(8):1328–1340. doi:10.1124/dmd.110.032326